Probing the Nature of the Redox Products and Lowest Excited State of $[(bpy)_2Ru(\mu\text{-}bptz)Ru(bpy)_2]^{4+}$: A Resonance Raman Study

Keith C. Gordon,*[a] Anthony K. Burrell,[b] Timothy J. Simpson,[a] Simon E. Page,[a] Geoffrey Kelso,[a] Matthew I. J. Polson,[a] and Amar Flood[a]

Keywords: Raman spectroscopy / Mixed-valent compounds / Ab initio calculations / Ruthenium(II) / Tetrazines

The resonance Raman and infrared spectra of the bridging ligand 3,6-bis(2-pyridyl)-1,2,4,5-tetrazine (bptz) have been studied. Ab initio calculations on bptz and the radical anion $bptz^{\cdot-}$ are able to predict the frequencies and intensities of the vibrational spectra. This analysis is used to interpret the vibrational spectroscopy of the bridged binuclear complexes $[(bpy)_2Ru(\mu\text{-}bptz)Ru(bpy)_2]^{4+}$ (**1**) and $[(PPh_3)_2Cu(\mu\text{-}bptz)Cu(PPh_3)_2]^{2+}$ (**2**) and their redox products. The resonance Raman spectroscopy of **1** reveals the bichromophoric nature of the complex, with bpy and bptz ligand modes being enhanced selectively as a function of excitation wavelength. The UV/Vis spectrum of $\mathbf{1}^+$ reveals a strong IVCT band suggesting the mixed-valent species is Class III in nature. This is consistent with findings for other metal moieties with the bptz ligand. The resonance Raman spectrum of $\mathbf{1}^+$ is also consistent with a Class III formulation. The resonance Raman spectrum of $\mathbf{2}^-$ is used to model $bptz^{\cdot-}$ and the ab initio calculations show some correlation with the observed spectrum. The excited-state resonance Raman spectra of **1**, generated with 532 and 633 nm excitation, show spectral features that are not strongly characteristic of $bptz^{\cdot-}$. This appears to be a consequence of the delocalised nature of the molecular orbitals involved in the excited-state of **1**.

Introduction

The extent to which different bridging ligands (BL) can facilitate coupling between adjacent metal-based moieties is an area of intense interest.[1−3] Mixed-valence complexes in which such metal coupling may occur are classified as Class I, II, or III. In a complex in which the BL provides no or little communication the resulting mixed-valent species would show Class I behaviour but when the communication is effective, Class II or III states may be formed.[4−8] Class III systems are completely delocalised such that the mixed-valence is equally shared by both metal centres. The Class II classification is intermediate between I and III, in which a barrier exists to moving charge between the adjacent centres. Studies of mixed-valence complexes may focus on the bridging ligand, by observing the properties of the π* MO.[9] The metal communication may be probed by creating mixed-valent species and observing inter-valence charge-transfer (IVCT) transitions, or by measuring the separation between metal-based oxidation for identical moieties such as $\{Fe(CN)_4\}^{2-}$ or $\{Ru(bpy)_2\}^{2+}$.[10−14] The electrochemical methods have been widely used to measure the comproportionation constant (K_c) for the mixed-valent species. Generally the mixed-valent species of interest is formed through chemical or electrochemical redox reactions.[15,16] However, it is possible to form mixed-valence species through photoexcitation of a binuclear metal complex:[17]

$$M-BL-M + h\nu \rightarrow M^+-BL^{\cdot-}-M \quad (1)$$

Fewer studies have addressed the nature of the mixed-valent state formed upon such excitation. Vibrational spectroscopy is a very powerful tool in this regard as reporter ligands may be used to provide vibrational signatures that are oxidation-state sensitive. The mixed-valent state may be accessed through electrochemistry[18−20] or photoexcitation.[17,21−26]

The aims of the present study are to probe the nature of the lowest excited state and the redox states of $[(bpy)_2Ru(\mu\text{-}bptz)Ru(bpy)_2]^{4+}$ (**1**) using resonance Raman spectroscopy. The structure of the bridging ligand, 3,6-bis(2-pyridyl)-1,2,4,5-tetrazine (bptz) is shown in Figure 1. The advantage of studying **1** is that the compound has a well-defined redox behaviour.[27,28] Thus the spectroscopic data obtained may

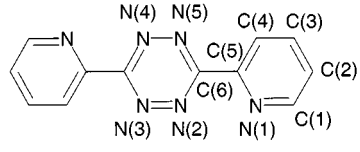

Figure 1. Structure and numbering system for bptz

[a] Chemistry Department, University of Otago, Union Place, Dunedin, New Zealand
Fax: (internat.) + 64-3/479-7906
E-mail: kgordon@alkali.otago.ac.nz
[b] IFS, Chemistry, Massey University, Palmerston North, Private Bag 11222, New Zealand

  1434−1948/02/0303−0554 $ 17.50+.50/0 *Eur. J. Inorg. Chem.* **2002**, 554−563

be related to a specific type of mixed-valent system, in this case Class III. The mixed-valent species formed by electrochemical oxidation is delocalised.[29] Furthermore the MO structure of the bridging ligand, bptz, has been studied experimentally[27] and through computational calculations.[30] These have found the redox MO for the reduced ligand and **1** to be strongly localised on the tetrazine portion of the bptz ligand. Complex **1** therefore provides a system in which each of the redox states that constitute an idealized model of the MLCT excited-state are known.

One of the disadvantages of using resonance Raman spectroscopy to probe the redox states and the lowest excited state of **1** is the presence of a number of overlapping chromophores in the visible region. In studying complexes with the $\{Ru(bpy)_2\}^{2+}$ moiety the strong enhancement of the bpy modes through the $Ru^{II} \rightarrow$ bpy MLCT transitions often conspire to obscure the resonance Raman spectral features from the other ligand present.[31–34] In order to obtain uncontaminated spectral signatures for bptz and bptz$^{\cdot-}$ the resonance Raman spectra of $[(PPh_3)_2Cu(\mu\text{-}bptz)Cu(PPh_3)_2]^{2+}$ (**2**) and **2**$^-$ were obtained. The $\{Cu(PPh_3)_2\}^+$ moiety possesses no additional chromophores in the visible region other than the $Cu^I \rightarrow$ bptz MLCT transition. Furthermore the $\{Cu(PPh_3)_2\}^+$ moiety causes only modest changes in the ligand structure and complexes with $\{Cu(PPh_3)_2\}^+$ may be used to obtain the radical anion spectra of ligands.[35–37] The crystal structures of **2**, reported herein, and **2**$^-$, previously published,[38] permit an analysis of the changes in the vibrational spectra in terms of the changes in bond lengths attendant upon reduction.

Results and Discussion

Electronic Spectroelectrochemistry

The electronic spectroscopic data for **1**, **2**, bptz, and their redox products are summarized in Table 1.

Table 1. Electronic absorption data for bptz, complexes, and their redox products

Compound	λ [nm] (ε [10^3 M^{-1}·cm^{-1}])				
bptz[a]	294 (19.6)				
bptz$^{\cdot-}$ [a]		368 (6.4)			
1[b]	281 (64.1)		404 (7.5)	688 (13.6)	
1$^+$ [b]			478 (4.6)	604 (12.2)	1483 (2.8)
1$^-$ [b]			434 (14.6)	491 (14.7)	
2[a]	258 (32.6)			707 (4.5)	
2$^-$ [a]			430 (3.7)		

[a] CH_2Cl_2 solution. [b] MeCN solution.

Reduction results in the depletion of ground state bands and the grow in of bptz$^{\cdot-}$ bands at approximately 400 to 450 nm. The spectra of **1**$^-$ and **2**$^-$ contain a bptz$^{\cdot-}$ band at ca. 430 nm. The spectrum of **1**$^-$ is also complicated by the red-shifting of $Ru^{II} \rightarrow$ bpy MLCT transitions as a consequence of the raising of dπ orbitals' energies because of the bptz reduction.[11] The spectrum of bptz$^{\cdot-}$ in solution shows a band at 368 nm. Recent studies of the spectroelectrochemistry for the mononuclear complex $[(bptz)Re(CO)_3Cl]^{\cdot-}$ reveals a band at 390 nm attributed to the bptz$^{\cdot-}$ species.[45a]

The absorption spectrum of **2** shows a strong MLCT transition at 707 nm. Reduction of **2** → **2**$^-$ results in the depletion of this band with the grow in of transitions at 430 and a shoulder at 520 nm, attributed to the radical anion of bptz. This is in good agreement with the reported UV/Vis spectrum of **2**$^-$ formed through comproportionation reaction,[38] which shows bands at 427 and 510 nm, and that observed for $[Cp^*ClIr(\mu\text{-}bptz)IrClCp^*]^+$ [39] which shows a band attributed to bptz$^{\cdot-}$ at 428 nm with ε = 4500 M^{-1} cm^{-1}.

The electrochemical oxidation of **1** → **1**$^+$ shows a reduction in the intensity of the MLCT band at 688 nm concomitant with the appearance of bands at 604 nm and 1483 nm (Figure 2). The intensity of the band in the NIR region is significantly greater than that observed for the related $[(NH_3)_4Ru(\mu\text{-}bptz)Ru(NH_3)_4]^{5+}$ (**3**$^+$).[30] In that case a band observed at 1453 nm (ε ≈ 500 M^{-1} cm^{-1}) was assigned as the IVCT transition. We propose that the feature observed at 1483 nm in **1**$^+$ is also of IVCT origin; however this band is more intense than that for the related **3**$^+$ complex. For both **1**$^+$ and **3**$^+$ the mixed-valent species formed are Class III in nature.[1,9] This may be established from the electrochemistry, the separation between metal-based oxidations being > 400 mV, and from the band shape of the IVCT band. In Class III systems the bandwidth ($\Delta\nu_{1/2}$) is less than that predicted by Hush theory.[7,8] In the Hush analysis the bandwidth is related to the transition wavenumber (ν) by $\Delta\nu_{1/2} = (2310\nu)^{1/2}$ cm^{-1}.

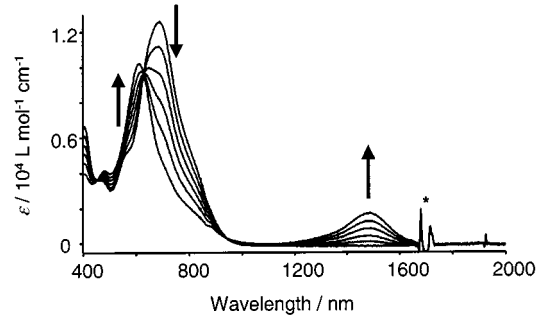

Figure 2. UV/Vis absorption spectra for **1** → **1**$^+$ (MeCN) electrochemical oxidation; arrows indicate the spectral changes occurring as the sample is oxidized; the asterisk * indicates overtone absorption bands of solvent (MeCN)

Compounds that show IVCT bands that fit this model are Class II in nature, whereas those which show much narrower transitions are Class III.[40]

For **1**$^+$ and **3**$^+$ the experimental values of $\Delta\nu_{1/2}$ are 1000 and 1600 cm^{-1},respectively, the values predicted through Hush theory would be 3960 and 3990 cm^{-1} for **1**$^+$ and **3**$^+$. They are therefore Class III systems. As **1**$^+$ and **3**$^+$ are Class III mixed-valence systems the amount of coupling may be parameterised by H_{ad}. This parameter represents the bonding interactions between the two identical Ru sites

directly and/or through superexchange pathways.[1,7,8] H_{ad} is related to the wavenumber of the IVCT transition (E_{op}) by $E_{op} = 2H_{ad}$.

In $\mathbf{1}^+$ and $\mathbf{3}^+$ H_{ad} is 3300 and 3440 cm^{-1}, respectively.

The upshot of this is that the μ-bptz ligand is allowing a similar level of coupling in the two complexes. The question arises as to why in $\mathbf{1}^+$ the IVCT transition is 5 times more intense than in $\mathbf{3}^+$. A similar phenomenon has been observed in mixed-valence complexes with 1,4-dicyanoamidobenzene.[41] In this case the peripheral ligands could tune the system between Class II and Class III behavior. The magnitude of the transition dipole moment (M) for the IVCT transition is dependent upon the overlap integral between the donor and acceptor wavefunctions (S_{ad}) and the dipole moment length (R).[40]

In the case of $\mathbf{3}^+$ the highly delocalised donor and acceptor wavefunction mean that R will be very small. This would result in a low ε for the IVCT band as is observed. In the case of $\mathbf{1}^+$ the dipole length is greater because of the inclusion of the bpy ligands in the donor and acceptor wavefunctions. Calculations on related Ru^{II} mononuclear complexes reveal that NH_3 ligands show less potential to mix with the dπ Ru^{II}-based HOMO than if bpy ligands are present.[42] In the case of $[Ru(bpy)_2L]^{2+}$ complexes the HOMO has ca. 70% dπ Ru character. In the case of $\mathbf{1}^+$ it is therefore reasonable to assume that the nature of the donor and acceptor MOs of the IVCT transition produce a greater dipole length than for $\mathbf{3}^+$.

Calculations of Structure and Crystal Structure Determination

The geometry of bptz was calculated by using HF and DFT (B3LYP) methods. In each case the ligand geometry was planar. Bond lengths and angles for the calculated and crystal structures are shown in Table 2. The notation is given in Figure 1. The result is surprising in view of the previously reported geometry optimization of bptz,[43] which reports a dihedral angle [as defined by N(1)−C(5)−C(6)−N(2)] of 19°. Furthermore, the crystal structure of the bptz contains a dihedral angle of 19°. In order to test our calculations we delibrately started the optimization with the structure having a significant dihedral angle. An analysis of the geometry optimization reveals that the major structural modification is in the dihedral angle − no other parameters show greater than 5% variation. Other than this discrepancy the bond lengths and angles we calculate are in good agreement with the crystal structure. Importantly the frequency calculations from these optimised structures show no imaginary frequencies, suggesting the geometries are at minimum energy.

An analysis of the bond lengths and angles reveals that the structure predicted at HF/6-31G(d) corresponds less closely to the crystal structure than the DFT (B3LYP) method. The average discrepancy in bond length for the HF calculation is 0.005 Å whereas for B3LYP it is 0.002 Å, for both basis sets used. The HF calculation generally does a poorer job with the C−N bond lengths and the N−N linkage is also too short. The increase in basis set in the B3LYP calculation does little to improve the predicted geometry.

Calculations were also carried out by using DFT methods on the radical anion of bptz. The spin expectation value, $<s^2>$, for the radical anion was 0.7501. This is very close to that for a pure doublet. We did not use HF methods to model the radical anion because they often give very poor $<s^2>$ values.[44] The calculated structure shows a lengthening of the N=N bond of the tetrazine. This is consistent with the population of a LUMO by the reducing electron that is based on the tetrazine and is antibonding with respect to the N=N bonds. It is consistent with the crystallographic data, vide infra.

The structure of **2** is similar to the previously described complexes, with the bptz acting as a linear bidentate ligand.[39,45] The structure confirms the presence of two $\{Cu(PPh_3)_2\}^+$ groups bound at a Cu−Cu distance of 6.78

Table 2. Bond lengths [Å] and angles [°] from calculations and crystallographic data

	bptz				**2**	$bptz^{\cdot-}$	$\mathbf{2}^-$
	Crystal structure[a]	HF/6-31G(d)	B3LYP/ 6-31G(d)	B3LYP/ 6-311G(d)	Crystal structure[b]	B3LYP/ 6-31G(d)	Crystal structure[c]
N(1)−C(1)	1.3326	1.316	1.333	1.330	1.350	1.340	1.338
C(1)−C(2)	1.388	1.382	1.398	1.396	1.376	1.400	1.385
C(2)−C(3)	1.381	1.386	1.393	1.391	1.372	1.400	1.375
C(3)−C(4)	1.387	1.384	1.393	1.390	1.400	1.393	1.381
C(4)−C(5)	1.3934	1.389	1.403	1.401	1.394	1.413	1.392
C(5)−N(1)	1.344	1.322	1.343	1.339	1.3495	1.361	1.353
C(5)−C(6)	1.4803	1.491	1.487	1.487	1.484	1.480	1.479
C(6)−N(5)	1.3416	1.323	1.348	1.345	1.3403	1.391	1.337
C(6)−N(2)	1.3426	1.323	1.348	1.345	1.3595	1.331	1.337
N(2)−N(3)	1.3198	1.285	1.315	1.311	1.334	1.399	1.393
C(4)−C(5)−N(1)	123.67	122.9	123.1	122.9	123.11	121.3	122.1
N(2)−C(6)−N(5)	124.77	123.1	124.1	123.9	125.1	127.0	129.9
N(1)−C(5)−C(6)−N(2)	19	0.00	0.00	0.00	9.72	0.00	0.00
Energy [Hartrees]		−785.68614	−790.51490	−790.68177		−790.55268	

[a] Ref.[43] [b] This work. [c] Ref.[38]

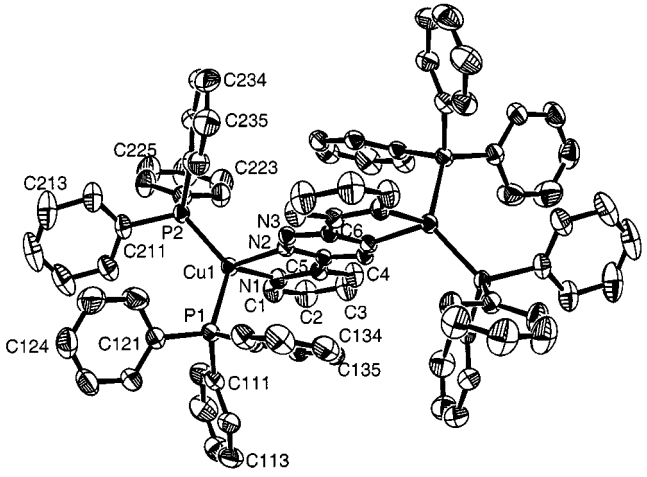

Figure 3. Molecular structure of **2** with thermal ellipsoids at 50% probability; selected bond lengths [Å]: Cu1−N2 2.0666(15), Cu1−N1 2.0957(17), Cu1−P2 2.2469(5), Cu1−P1 2.2760(5), N2−N3 1.329(2), N2−C6′ 1.355(2), N3−C6 1.341(2)

Å, Figure 3. The bond length and angles for the bptz moiety are presented in Table 2. The geometry about the copper is not completely tetrahedral with the small bite-angle of the bptz ligand and an axial-equatorial displacement of the PPh_3 groups. This displacement is not unusual in complexes of this type[46] and is driven by the π−π interactions between the tetrazine ring and one of the phenyl rings on each PPh_3. The distance from the tetrazine to the phenyl range from 3.3−3.7 Å.

The structure of the reduced complex has been previously reported and it is useful to compare the two structures in some detail. The structural details for bptz in **2** and $\mathbf{2}^-$ are given in Table 2.[38] The most important area for comparison is the bond lengths in the tetrazine ring. The study by Kaim and co-workers indicated that the reducing electron was located in the π* orbital of the N=N bond. The structure of **2** helps support this proposal; the N=N distance [1.329(2) Å] is significantly shorter than that observed in $\mathbf{2}^-$ [1.394(5) Å]. The other distances in the tetrazine ring of **2** do not vary significantly from those described in $\mathbf{2}^-$ (see Table 2). The bptz ligand in **2** is slightly more distorted than its anion radical form $\mathbf{2}^-$. The twist angle between the pyridyl groups and the tetrazine ring in **2** is 7.69°, whereas it is only 5.8° in $\mathbf{2}^-$. Another notable distortion is caused by the coordination of Cu^I. The ligand gains a slight distortion which can be seen in the relative distances between N1−N2 (2.66 Å) and N4−C4 (2.98 Å). The Cu−N distances show the same trend for **2** as noted for $\mathbf{2}^-$ with the Cu−N(1) pyridyl bond [2.0957(17) Å] being longer than the Cu−N(2) tetrazine [2.0666(15) Å] bond. The Cu−P distances in **2** at 2.2469(5) and 2.2760(5) Å are relatively similar, whereas in $\mathbf{2}^-$ they differ significantly [2.0297(12) and 2.2873(12) Å].

Frequency Calculations and Resonance Raman Spectroscopy

The frequency calculations were performed on bptz within a C_{2h} point group. The energy difference between the bptz with no symmetry and that with C_{2h} is less than $1.2\cdot10^{-7}$ Hartrees ($3.1\cdot10^{-1}$ J·mol^{-1}). Essentially the structures are equivalent.[47]

The frequencies calculated at HF/6-31G(d) were empirically scaled by 0.87 according to the findings of Radom et al.[48] The IR intensities and Raman activites were also obtained. Frequencies were also calculated using the DF hybrid method [B3LYP with a 6-31G(d) basis set, frequencies were scaled by 0.96].[48] The IR and Raman intensities were also calculated.

The HF and DFT calculations show reasonably good agreement with the IR data. The difference between the frequency calculations at HF and DFT/B3LYP level in the 1100 to 1700 cm^{-1} region are that the HF calculation poorly predicts the intensities of the Raman spectrum. It also places more a_g modes above 1500 cm^{-1} than the DFT calculation and has only two modes in the 1400 to 1500 cm^{-1} region. The Raman spectrum of bptz clearly shows 3 bands in the 1400 to 1500 cm^{-1} region. Furthermore the intensities calculated from HF predict strong Raman bands in the 1530 and 1600 cm^{-1}. This is not observed in the experimental spectra. For these reasons the HF calculations are not used in our subsequent analyses.

A listing of modes, their symmetries and wavenumbers for the DFT calculation and experimental data are given in Table 3.

The measured IR spectrum of bptz shows strong transitions at 1586, 1387, and 1130 cm^{-1} (Table 3). These correspond to modes 64, 54, and 45, respectively, from the DFT calculation. These modes are depicted in Figure 4 and can be best described as being pyridine ring (mode 64) and tetrazine ring (modes 54 and 45) stretches.

The Raman activity is related to the intensity of Raman bands as a function of the excitation wavelength and the wavenumber of the Raman photon.[49] It should be noted that the spectrum of bptz is a resonance Raman spectrum and this affords enhancement of band intensities not simply related to the Raman scattering cross section as calculated in the simulated spectrum. A detailed quantitative analysis is therefore inappropriate. It should, however, be noted that a_g modes are enhanced in resonance Raman spectra.[50] The predicted modes that should show large Raman scattering cross section are at 1599 (mode number 63), 1461 (mode 57), 1322 (mode 52), and 1278 cm^{-1} (mode 49). Modes 57 and 52 are almost exclusively tetrazine based stretches (Figure 4).

The calculated spectra of $bptz^{\cdot-}$ were only run using DFT methods. The predicted frequencies and intensities for $bptz^{\cdot-}$ are presented in Table 4. The Raman spectrum in the 1100 to 1700 cm^{-1} is dominated by mode 56 at 1380 cm^{-1}. This mode corresponds to mode 57 for the neutral ligand. A number of other weak a_g modes are also Raman-active in the 1100 to 1700 cm^{-1} region. It is interesting to note that those bands that are associated with normal modes of pyridine-ring character, such as modes 64 and 63, are predicted not to shift much upon reduction. However, the tetrazine modes, such as 57, 54, and 52, are predicted to shift significantly. Mode 57 (1461 cm^{-1} for bptz) is pre-

Table 3. Wavenumbers [cm^{-1}] of experimental and calculated bands for bptz in the 1000 to 1650 cm^{-1} region

bptz B3LYP/6-31G(d) calculated			bptz experimental data	
Mode number	Mode symmetry	ν [cm^{-1}][a]	IR ν [cm^{-1}][b]	Raman ν [cm^{-1}][c]
38	b_u	995 (9, 0)	993 (17)	
39	a_g	1034 (0, 1)		
40	b_u	1042 (2, 0)	1042 (8)	
41	b_u	1052 (6, 0)		
42	a_g	1067 (0, 0)		
43	b_u	1097 (2, 0)	1092 (5)	
44	a_g	1099 (0, 0)		
45	b_u	1132 (32, 0)	1130 (36)	
46	b_u	1156 (0, 0)	1152 (27)	
47	a_g	1156 (0, 1)		
48	b_u	1256 (1, 0)	1241 (7)	
49	a_g	1278 (0, 25)		1266
50	b_u	1291 (22, 0)	1255 (1)	
51	a_g	1291 (0, 0)		
52	a_g	1322 (0, 14)		1314
53	b_u	1339 (2, 0)		
54	b_u	1388 (100, 0)	1387 (100)	
55	a_g	1430 (0, 5)		1447
56	b_u	1448 (6, 0)	1444 (10)	
57	a_g	1461 (0, 100)		1462
58	a_g	1471 (0, 1)		1476
59	b_u	1485 (1, 0)		
60	a_g	1495 (0, 0)		
61	b_u	1589 (12, 0)	1576 (10)	
62	a_g	1590 (0, 0)		1576
63	a_g	1599 (0, 26)		1591
64	b_u	1599 (7, 0)	1586 (19)	

[a] Relative intensities of IR and Raman bands, respectively, are given in parentheses. The band intensities are normalized so that the strongest band in the reported region has an intensity of 100. [b] Relative intensities given in parentheses; normalized to 100 for the strongest band in the region. [c] These data pertain to a resonance Raman spectrum. The intensities are modulated by the resonance effect, hence they are not comparable to the predicted spectra and are not given.

dicted to shift to 1380 cm^{-1} in $bptz^{\cdot -}$ (corresponding to mode 56). Mode 54 shifts from 1388 to 1328 cm^{-1} and mode 52 from 1322 to 1280 cm^{-1}. These shifts are consistent with population of a tetrazine-based MO in $bptz^{\cdot -}$ and the concomitant weakening of the N−N linkages.

The resonance Raman spectra (RRS) of the complexes are presented in Figure 5.

The Raman spectrum of the bptz ligand (Figure 5, bptz) shows strong bands at around 1447 cm^{-1} and at 1591 and 1576 cm^{-1}. The 1447 cm^{-1} group of modes are assigned as predominantly tetrazine ring stretch, those at higher frequency are pyridyl ring stretches. If the excitation wavelength is changed from 457.9 nm to 514.5 nm the relative intensity of the 1447 cm^{-1} is diminished suggesting resonance enhancement of these spectra. All of the observed bands are polarised and are thus from modes of a_g symmetry.

The binding of the two $\{Ru(bpy)_2\}^{2+}$ moieties results in more complex resonance Raman spectra (Figure 5; **1**). The complex has two sets of chromophores in the visible region; these are Ru(dπ) → bpy(π*) MLCT transitions and Ru(dπ) → bptz(π*) MLCT transitions. From electrochemical studies the bptz-terminated MLCT transition should lie at lower energy than the bpy-based MLCT band. This is borne out in the resonance Raman spectra where bpy modes at 1605, 1566, 1499, 1317, and 1172 cm^{-1} are very strong with 457.9 nm excitation (Figure 5; **1**, 457 nm).[33] Modes associated with the bptz ligand lie at 1503 and 1366 cm^{-1} and are attributed to modes 60 and 53. The intensity of the 1366 cm^{-1} is convoluted with the solvent band; it is therefore difficult to assign. The observed bptz bands of **1** are significantly shifted from the bands in the free ligand. This may be due to the electronic effect of the $\{Ru(bpy)_2\}^{2+}$ distorting the ligand, or its steric effect. The relative intensity of the bpy modes is depleted as the excitation wavelength is tuned from 488.0 to 514.5 to 632.8 nm. With the red excitation wavelength no bpy modes are observed suggesting the Ru → bpy MLCT transition has negligible intensity at this wavelength.

The RRS of **2** (Figure 5) shows the enhancement of modes at 1488, 1459, 1437, 1305, and 1290 cm^{-1} assigned as modes 60, 57, 55, 52, and 51. For bptz they are shifted slightly from the Raman bands of the free ligand.

The RRS of **1** and **2** are generally similar with 632.8 nm excitation; they both show a strong band at about 1490 cm^{-1}, 1488 for **2** and 1503 cm^{-1} for **1**, and a group of vibrations at about 1300 cm^{-1}. The wavenumbers are shifted significantly for each. Structural data are not available for **1** but recent detailed calculations on related Pt^{II} complexes reveal significant perturbation of the electronic structure of bptz by the bound metals.[43] It is known that the $\{Ru(bpy)_2\}^{2+}$ moiety is a stronger π-acid than $\{Cu(PPh_3)_2\}^{+}$ and this may lead to perturbations of the ring structure and thus the vibrational spectra of the ligand.

Resonance Raman Spectroelectrochemistry

Resonance Raman spectroelectrochemistry offers a vibrational spectroscopic probe of the mixed-valent state, with oxidation, and of the bptz radical anion species, with reduction. The latter has already been thoroughly studied using ESR spectroscopy.[51] Such studies revealed that most of the electron density in the MO populated in the reduced species is localised at the tetrazine ring.

The resonance Raman spectrum of $\mathbf{1}^{+}$ was measured using 457.9, 488.0, 514.5, and 632.8 nm excitation wavelengths (Figure 5). In ascertaining the electron density changes about a metal upon oxidation, reporter groups are often utilised. These may be CO or CN^{-} ligands; both show a sensitivity of wavenumber of the stretch vibration to the oxidation state of the metal atom.[17,21−23] However, the bpy vibrations are also frequency dependent on the oxidation state of the metal atom.[33,34] For $[Ru(bpy)_3]^{3+}$ the bpy modes lie approximately 3−5 cm^{-1} higher in frequency than observed in the vibrational spectrum of $[Ru(bpy)_3]^{2+}$.[52] The spectra observed for $\mathbf{1}^{+}$ show bpy bands that are slightly shifted from that of **1**. This is most readily observed in the spectrum generated with 457.9 nm excitation; the bpy band at 1605 cm^{-1} in **1** is shifted to 1608 cm^{-1} in $\mathbf{1}^{+}$. Although this is a small shift it is not negligible

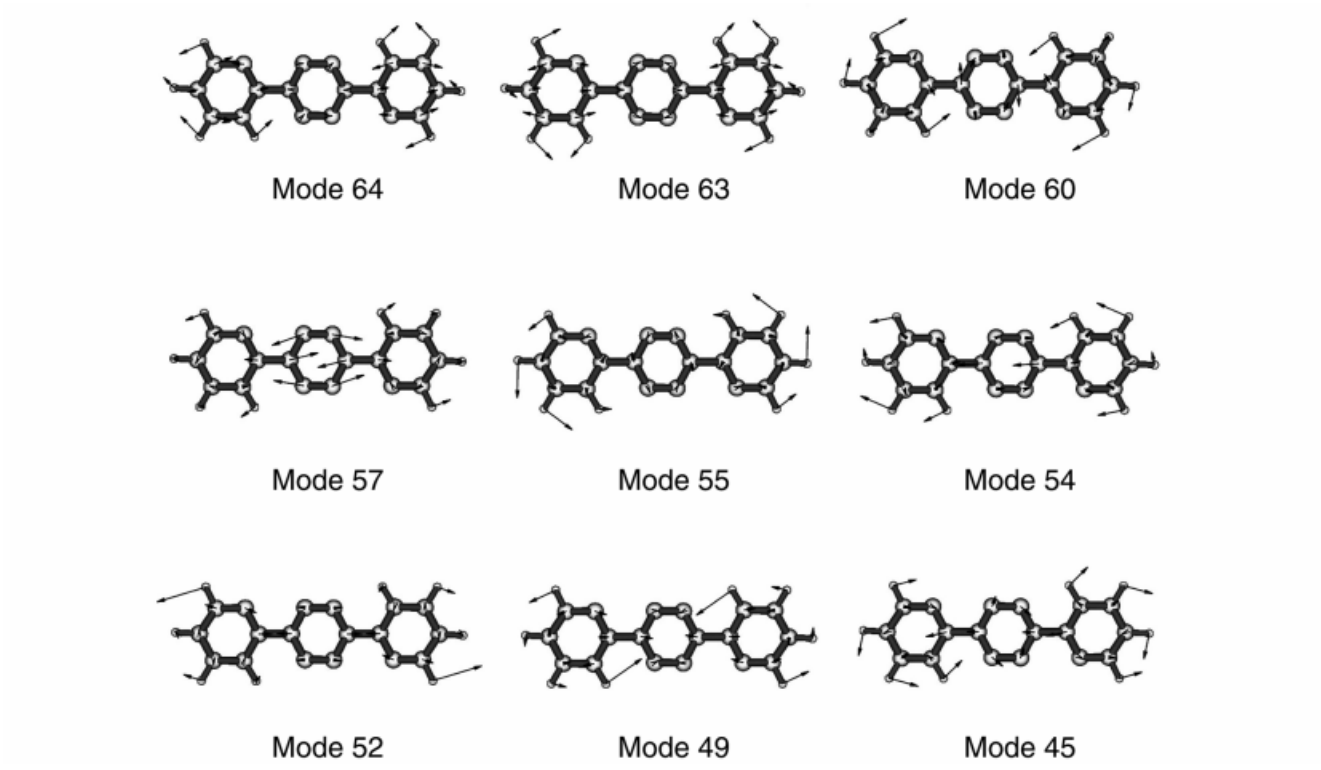

Figure 4. Selected normal modes calculated for bptz. Modes 64 and 63 are pyridine-based, 57, 54, and 52 are tetrazine-based

and is consistent with oxidation of a metal site or sites. The largest frequency shift observed in comparing **1** and $\mathbf{1}^+$ is the bptz band at 1503 and 1513 cm^{-1} respectively. This is most readily seen in the spectra generated with 632.8 nm excitation. The significance of these data are as follows: (1) The larger shift for the bptz vibrational transition is consistent with significant perturbation at the bridging ligand relative to the peripheral bpy ligands. (2) The shift of the bpy mode upon oxidation is consistent with a perturbation of electron density at *both metal sites*; an unperturbed Ru^{II} centre would retain bpy signatures at 1605 cm^{-1}. This is perhaps unsurprising in view of the strong coupling between the metal sites.[45a] Oxidation is likely to create an $\{Ru^{+2.5}(\mu\text{-bptz})Ru^{+2.5}\}$ species; thus the electron density change on the metal atoms is delocalised and changes in the bonding of the bpy ligands is delocalised over both metal centres.

The 10 cm^{-1} frequency shift of the bptz band, in relation to point (1) above, provides support for the presence of a superexchange contribution to the production of a Class III species. Consequently, the HOMO has some bptz π-character, in which the $\mathbf{1}^+$ formulation $\{Ru^{+2.4}(bptz^{+0.2})Ru^{+2.4}\}$ may be more truthfully representative. That is, the 10 cm^{-1} frequency shift of the bptz band is a direct result of the depopulation of the HOMO which is constituted by some% of bptz π-character.

In summary, the resonance Raman spectroscopy of $\mathbf{1}^+$ is consistent with a Class III species.

The electrochemical reduction of $\mathbf{2} \rightarrow \mathbf{2}^-$ results in significant spectral changes; firstly, the RRS of $\mathbf{2}^-$ is much more intense than that of **2** generated with 457.9 nm excitation. A new set of bands are observed at 1406, 1313, 1274, 1027, and 1002 cm^{-1}. These may be assigned to modes 56, 53, 51 43, and 40, respectively. The correlation is based on: (1) the fact that this is a resonance Raman spectrum, thus a_g modes will be enhanced; (2) the calculation predicts some intensity for each. The strongest of these bands lie at 1406 and 1274 cm^{-1}. The crystal structure of $\mathbf{2}^-$, and calculations on $bptz^{\cdot -}$, reveal that the N=N bond is 1.39 Å in $\mathbf{2}^-$ and 1.32 Å in **2**. The shift to lower frequencies is most prevalent for the tetrazine modes as predicted by calculation.

The resonance Raman spectra of $\mathbf{1}^-$ show significant changes to those of the parent complex at all 4 excitation wavelengths (Figure 5). The spectrum of $\mathbf{1}^-$ generated with 457.9 nm excitation shows bands at 1506 cm^{-1} that may be assigned as a $bptz^{\cdot -}$ feature; other bands at 1605, 1486 and 1317 cm^{-1} are bpy modes. Complete conversion from the parent species is confirmed by the absence of any residual 1494 cm^{-1} band. The band at 1559 cm^{-1} (mode 62, Table 4) is rather interesting; it appears to be composed of bpy and $bptz^{\cdot -}$ vibrations. The spectrum at 488.0 nm excitation shows similar bands with the bpy-modes reduced in intensity. However, their relative intensity is greater in the spectrum of $\mathbf{1}^-$ than in that of **1** at the same excitation wavelength. This is consistent with a destabilisation of the metal t_{2g} MOs upon reduction at the ligand site. This effect redshifts the $Ru(d\pi) \rightarrow bpy(\pi^*)$ MLCT transitions causing them to become resonant at 488.0 and 514.5 nm.[33,34,53]

The resonance Raman spectrum of $\mathbf{1}^-$ observed with 632.8 nm excitation shows a very different intensity pattern than that observed at the other excitation wavelengths. Firstly, no bpy modes are observed. This is consistent with

Table 4. Wavenumbers [cm^{-1}] of calculated bands for bptz$^{\cdot-}$, and experimental bands of $\mathbf{2}^-$ in the 1000 to 1650 cm^{-1} region

bptz$^{\cdot-}$ B3LYP/6-31G(d) calculated data			Resonance Raman data for $\mathbf{2}^-$
Mode number	Mode symmetry	ν [cm^{-1}][a]	ν [cm^{-1}][b]
41	b_u	1043 (51, 0)	
42	b_u	1049 (2, 0)	
43	a_g	1049 (0, 1)	1027
44	b_u	1083 (16, 0)	
45	a_g	1088 (0, 1)	
46	b_u	1134 (90, 0)	
47	a_g	1141 (0, 0)	
48	b_u	1143 (32, 0)	
49	a_g	1230 (0, 2)	
50	b_u	1261 (29, 0)	
51	a_g	1280 (0, 1)	1274
52	b_u	1283 (17, 0)	
53	a_g	1303 (0, 0)	1313
54	b_u	1328 (20, 0)	
55	b_u	1361 (34, 0)	
56	a_g	1380 (0, 1000)	
57	a_g	1435 (0, 3)	1406
58	b_u	1435 (70, 0)	
59	a_g	1477 (0, 0)	
60	b_u	1477 (66, 0)	
61	b_u	1574 (37, 0)	
62	a_g	1575 (0, 3)	
63	b_u	1593 (100, 0)	
64	a_g	1593 (0, 4)	

[a] Relative intensities of IR and Raman bands, respectively, are given in parentheses. The band intensities are normalized so that the strongest band in the reported region has an intensity of 100 for IR and 1000 for Raman. [b] These data pertain to a resonance Raman spectrum. The intensities are modulated by the resonance effect, hence they are not comparable to the predicted spectra and are not given.

the fact that at 632.8 nm there are no electronic transitions involving the bpy ligands. Secondly, the bptz$^{\cdot-}$ mode at 1559 cm^{-1} is absent and bands appear at 1005, 1257, and 1308 cm^{-1} in a pattern completely different from that observed at the other excitation wavelengths. The frequency calculation predicts modes at 996, 1280, and 1303 cm^{-1} which correspond to modes 40, 51, and 53, respectively. The enhancement of these modes is quite different from that observed for $\mathbf{2}^-$ (Figure 5; $\mathbf{2}^-$, 457 nm) and this suggests that the bptz$^{\cdot-}$ species has a number of transitions in the visible region that involve quite different portions of the bptz$^{\cdot-}$ radical anion ligand. This is also supported by the fact that the resonance Raman spectra of **2** show strong variations in intensity for bands at 1488 and 1305 cm^{-1} with λ_{exc} (Figure 5).

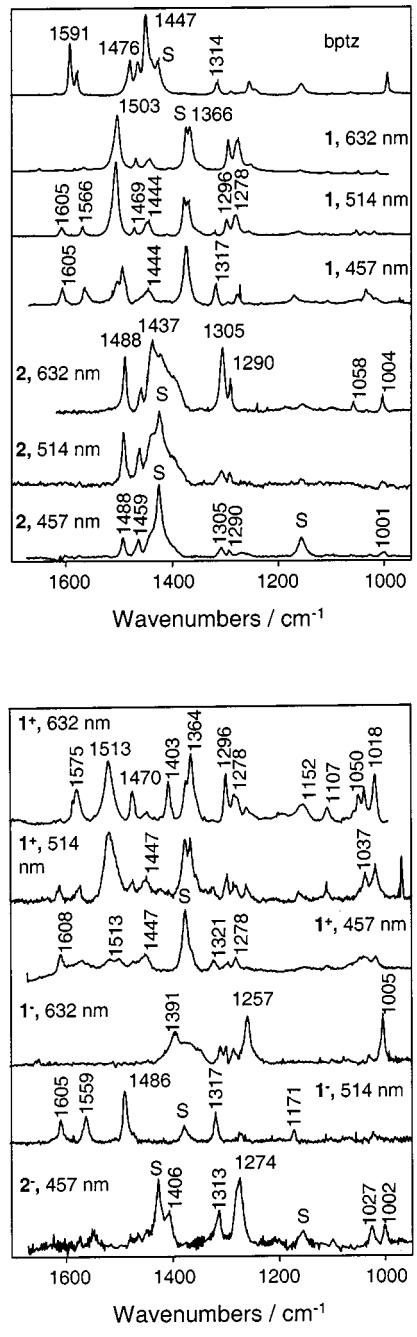

Figure 5. Resonance Raman spectra of **1** (3 mM MeCN), **2** (3 mM CH_2Cl_2), $\mathbf{1}^+$ (3 mM MeCN), $\mathbf{2}^-$ (3 mM CH_2Cl_2), $\mathbf{1}^-$ (3 mM MeCN); **S** represents a solvent band; all λ_{exc} = 15 mW at sample

Excited-State Resonance Raman Spectra

The excited-state lifetime of **1** has not been reported; the lack of any emission in fluid media suggests it is < 5 ns. It is possible to probe such short-lived species using nanosecond pulsed laser excitation at sufficient pump powers.[37,54–56] The RRS of **1** generated using 532 and 633 nm pulsed excitation are shown in Figure 6. As the pulse energy is increased a number of bands become stronger; these are assigned to the excited state (**1***). They lie at 988, 1100, 1120, 1161, 1568, and 1608 cm^{-1}. In a simple fashion the spectrum of **1*** can be thought of as a combination of the spectra of $\mathbf{1}^+$ and $\mathbf{1}^-$. The 1568 and 1608 cm^{-1} bands may be attributed to bpy vibrational bands of a Ru→bpy MLCT transition from an Ru centre. None of the other excited-state features present are bptz-associated marker bands for $\mathbf{1}^+$ or bptz$^{\cdot-}$ as probed in $\mathbf{1}^-$ or even $\mathbf{2}^-$.[57] This is in contrast to what is normally observed in the spectra of mononuclear polypyridylmetal complexes.[21,22] A plausible explanation for this discrepancy is that there is strong mixing

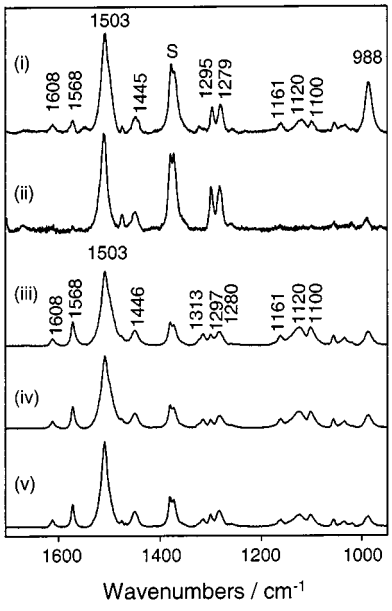

Figure 6. Resonance Raman spectra of **1** (2 mM MeCN) with pulsed laser excitation: (i) λ_{exc} = 633 nm, pulse energy 2 mJ; (ii) λ_{exc} = 633 nm, pulse energy 0.4 mJ; (iii) λ_{exc} = 532 nm, pulse energy 4 mJ; (iv) λ_{exc} = 532 nm, pulse energy 2 mJ; (v) λ_{exc} = 532 nm, pulse energy 0.5 mJ

(superexchange pathway) between the dπ and bptz π* MOs such that both the acceptor and donor orbital in the excited state are delocalised over the two Ru centres and bptz. Consequently, the bptz vibrational band positions will reflect the bonding changes due to the acceptor *and* donor orbitals and not solely the acceptor orbital as is the case for mononuclear metal polypyridyl complexes or Class I/II binuclear polypyridylmetal complexes. Therefore, the excited-state resonance Raman spectra of **1** are not inconsistent with a Class III formulation of the $\mathbf{1}^+$ mixed-valent state in which the Class III state is produced from a superexchange pathway via bptz.

Conclusion

Ab initio calculations can provide useful insight into the structure and vibrational spectra of ligands and their radical anions. In this case DFT calculations modelled the IR spectrum of bptz very well. The frequency calculation also allowed for a clear picture of the resonance Raman spectra of **1** and **2**.

The calculations on the $bptz^{\cdot-}$ predict a significant lengthening of the N=N linkage from 1.31 to 1.40 Å. This is the largest structural change predicted from the calculations. The crystal structure of $\mathbf{2}^-$ shows this predicted effect. The frequencies calculated for $bptz^{\cdot-}$ predict significant shifting of tetrazine modes from 1461 cm^{-1} in bptz (mode 57) to 1380 cm^{-1} in $bptz^{\cdot-}$ (mode 56). This may be correlated with bands of **2** at 1462 cm^{-1} shifting to 1406 cm^{-1} in $\mathbf{2}^-$.

The UV/Visible spectra of the oxidised complex, $\mathbf{1}^+$, shows a distinct and narrow IVCT transition at 1483 nm. This is somewhat more intense than that observed for other mixed-valent species with the bptz bridging ligand. We attribute the increased intensity to the ability of the $\{Ru(bpy)_2\}^{2+}$ moiety to mix bpy character into the wavefunction of the donor MO in the IVCT transition. This has the effect of increasing the dipole length of the transition and thus its intensity. The resonance Raman spectra of $\mathbf{1}^+$ reveal small shifts in the bpy bands consistent with metal oxidation. The absence of a discrete set of bpy bands for Ru^{II} and Ru^{III} centres suggests a Class III mixed-valent formulation for $\mathbf{1}^+$; consistent with previous findings.

The resonance Raman spectra of the complexes **1** and **2** are consistent with the UV/Vis spectral assignments. The resonance Raman spectra of **1** show enhancement of bpy modes at blue excitation wavelengths with bptz modes being enhanced with red excitation. This is consistent with Ru→bpy MLCT and Ru→bptz MLCT transitions. For **2** only bptz modes are enhanced with visible excitation. The change in relative intensities for the bptz bands suggest the presence of two Cu→bptz MLCT transitions in the visible region. This is exemplified by the increased resonance enhancement of the 1305 cm^{-1} band relative to 1488 cm^{-1} on going from 457.9 to 632.8 nm excitation.

The UV/Vis spectrum of $\mathbf{1}^-$ shows chromophores associated with the Ru→bpy MLCT and $bptz^{\cdot-}$ π→π* transitions. The spectra generated with 457.9, 488.0, and 514.5 nm excitation are dominated by bpy bands but at 632.8 nm excitation $bptz^{\cdot-}$ bands are evident. The signature for the $bptz^{\cdot-}$ comes from the spectrum of $\mathbf{2}^-$ which shows the vibrational signature of $bptz^{\cdot-}$ and reveals the π→π* transition to lie at ca. 430 nm.

The excited-state resonance Raman spectra of **1*** show spectral features that are not a simple linear combination of the oxidised metal centre and ligand radical anion. This is consistent with a pair of acceptor and donor orbitals that are delocalised over the two Ru centres and the bptz ligand. A delocalised donor orbital is consistent with a Class III mixed-valent species. It may also be due to the differing probe wavelengths employed in the excited-state spectra of **1** over the spectroelectochemical spectra of $\mathbf{2}^-$.

Experimental Section

Complex Synthesis: $[(bpy)_2Ru(\mu\text{-bptz})Ru(bpy)_2](PF_6)_4$ [**1**·$(PF_6)_4$] and $[(PPh_3)_2Cu(\mu\text{-bptz})Cu(PPh_3)_2](BF_4)_2$ [**2**·$(BF_4)_2$] were prepared by literature procedures.[58−60] Purity was confirmed by microanalysis. **1** can exist in a number of diastereoisomers; no attempt was made to separate them.

Physical Measurements: Electronic absorption spectra were measured using a Perkin−Elmer λ-19 spectrometer. Electrochemical and spectroscopic measurements used solvents of spectroscopic grade. These were further purified by distillation and were stored over 5-Å molecular sieves. The supporting electrolytes used in the electrochemical measurements were tetrabutylammonium perchlorate (TBAP) and tetrabutylammonium hexafluorophosphate (TBAH). These were purified by repeated recrystallizations from ethanol/water, for TBAP, or ethyl acetate/ether, for TBAH.[61] Cyclic voltammograms (CVs) were obtained from argon-purged degassed so-

lutions of compound (ca. 1 mM) with 0.1 M concentration of TBAP or TBAH present. The electrochemical cell consisted of a 1.6 mm diameter platinum working electrode embedded in a Kel-F cylinder with a platinum auxiliary electrode and a saturated potassium chloride calomel reference electrode. The CV was calibrated against ferrocene/ferrocenium couple by addition of ferrocene to the sample cell and the running of a calibration CV. The potential of the cell was controlled by an EG&G PAR 273A potentiostat with Model 270 software. Resonance Raman spectra, generated with continuous wave excitation, were obtained using an air-cooled argon ion laser (Melles−Griot Omnichrome 543-MAP) or helium-neon laser (Oplectra). Plasma emission lines were removed from the exciting beam using bandpass filters or a wavelength-specific holographic laser bandpass filter (Kaiser Optical Systems, Inc.). Spectra were analysed by using GRAMS 5.0 (Galactic Industries). The cell used for Raman spectroelectrochemistry was an OTTLE cell.[62] The sample was held in a spinning NMR tube or OTTLE cell and Raman photons were imaged into the spectrograph (SPEX 750M) with a 135° backscattering arrangement. The spectrograph was equipped with an 1800 g/mm holographic grating; detection was achieved using a CCD (Princeton Instruments 1152 EUV LN_2 cooled with CSMA version 2.3 software). Calibration of Raman spectra were achieved with neon or argon ion emission lines. Spectral calibrations were checked against solvent spectra.[63] This revealed that peak reproducibility was accurate to 1.5 cm^{-1} across differing excitation wavelengths. For electronic absorption spectroelectrochemistry spectra were acquired at a series of applied potentials stepping through the oxidation or reduction of interest. For Raman studies the applied potential was set beyond the $E^{0\prime}$ value of the electrochemical process, and data were collected after sufficient time that the probed volume contained only the reduced or oxidised product. The frequency-doubled output from an Nd:YAG (Continuum Surelite I-10) pulsed laser (5−7 ns pulse width, operating at 10 Hz) was used to generate excited-state resonance Raman (ESRR) spectra at 532 nm, it was also used to provide stimulated Raman scattering[64,65] for the ESRR experiments with 633 nm excitation. The 532 nm output from the Nd:YAG laser was focused into a 10-cm cell filled with spectrophotometric grade acetonitrile. A quartz Pellin−Broca prism was used to separate the co-linear partially depleted pump beam and four Stokes orders of stimulated Raman scattering. The first Stokes output from the Raman shifter was directed onto the sample in the same manner as the continuous-wave Raman experiments. Typically a 532 nm, 7−40 mJ pump pulse was used, generating 0.5−4.5 mJ of the second Stokes-shifted line at 633 nm. Beam diameter at sample was 300 μm. The geometry and vibrational frequencies of the bptz ligand and its radical anion were obtained using HF and DFT-HF hybrid calculations implemented with the Gaussian98 and -94 program packages.[66,67] Visualization of the MOs and vibrational modes was provided by the Molden package.[68]

X-ray Crystallographic Study: Crystal data for **2**·$(BF_4)_2$·CH_2Cl_2: $C_{85}H_{68}B_2Cl_2Cu_2F_8N_6P4$, M = 1668.93, triclinic, a = 13.2173(2), b = 13.2183(2), c = 14.70050(10) Å, α = 87.8200(10), β = 69.1300(10), γ = 64.0130(10)°, V = 2135.72(5) $Å^3$, T = 175 K, space group $P\bar{1}$, Z = 1, μ(Mo-K_α) = 0.699 mm^{-1}, d = 1.298 Mg/m^3. Data collection: Siemens SMART CCD area detector, graphite monochromator, 0.38 × 0.22 × 0.14 mm, 20511 reflections measured, 9168 unique (R_{int} = 0.0173) which were used in all calculations. The final $Rw(F_o^2)$ = 0.0983 [$R(F_o)$ = 0.0383] $Rw(F_o^2)$ = $[\{w(F_o^2 - F_c^2)^2\}]/\{w(F_o^2)^2\}]^{1/2}$ where w^{-1} = $[\sigma^2(F_o^2) + (aP)^2 + bP]$ (a = 0.0498; b = 1.20) and P = $[\max(F_o^2,0) + 2F_c^2]/3$. All other aspects of data collection, reduction, solution and refinement were performed as previously described.[62][69] Crystallographic data (excluding structure factors) for the structure(s) reported in this paper have been deposited with the Cambridge Crystallographic Data Centre as supplementary publication no. CCDC-166062. Copies of the data can be obtained free of charge on application to CCDC, 12 Union Road, Cambridge CB2 1EZ, UK [Fax: (internat.) + 44-1223/336-033; E-mail: deposit@ccdc.cam.ac.uk].

Acknowledgments

Support from the New Zealand Lottery Commission and the University of Otago Research Committee is gratefully acknowledged. A. F. would like to acknowledge the Alliance Group for a postgraduate scholarship.

[1] S. F. Nelsen, *Chem. Eur. J.* **2000**, *6*, 581−588.
[2] K. D. Demadis, G. A. Neyhart, E. M. Kober, T. J. Meyer, *J. Am. Chem. Soc.* **1998**, *120*, 7121−7122.
[3] K. D. Demadis, E.-S. El-Samanody, G. M. Coia, T. J. Meyer, *J. Am. Chem. Soc.* **1999**, *121*, 535−544.
[4] M. B. Robin, P. Day, *Adv. Inorg. Radiochem.* **1967**, *10*, 247−422.
[5] J. H. Elias, R. S. Drago, *Inorg. Chem.* **1972**, *11*, 415−418.
[6] R. W. Callahan, G. M. Brown, T. J. Meyer, *Inorg. Chem.* **1975**, *14*, 1443−1453.
[7] N. S. Hush, *Prog. Inorg. Chem.* **1967**, *8*, 391−444.
[8] N. S. Hush, *Coord. Chem. Rev.* **1985**, *64*, 135−157.
[9] C. Creutz, *Prog. Inorg. Chem.* **1983**, *30*, 1−73.
[10] H. Hartmann, T. Scheiring, J. Fiedler, W. Kaim, *J. Organomet. Chem.* **2000**, *604*, 267−272.
[11] T. Scheiring, W. Kaim, J. A. Olabe, A. R. Parise, J. Fiedler, *Inorg. Chim. Acta* **2000**, *300*, 125−130.
[12] M. Glockle, W. Kaim, *Angew. Chem. Int. Ed.* **1999**, *38*, 3072−3074.
[13] M. Ketterle, W. Kaim, J. A. Olabe, A. R. Parise, J. Fiedler, *Inorg. Chim. Acta* **1999**, *291*, 66−73.
[14] M. Ketterle, J. Fiedler, W. Kaim, *Chem. Commun.* **1998**, 1701−1702.
[15] S. D. Ernst, V. Kasack, W. Kaim, *Inorg. Chem.* **1988**, *27*, 1146−1148.
[16] S. Barlow, D. O'Hare, *Chem. Rev.* **1997**, *97*, 637−669.
[17] M. W. George, F. P. A. Johnson, J. J. Turner, J. R. Westwell, *J. Chem. Soc., Dalton Trans.* **1995**, 2711−2718.
[18] C. G. Atwood, W. E. Geiger, *J. Am. Chem. Soc.* **2000**, *122*, 5477−5485.
[19] T. Ito, T. Hamaguchi, H. Nagino, T. Yamaguchi, J. Washington, C. P. Kubiak, *Science* **1997**, *277*, 660−663.
[20] T. Ito, T. Hamaguchi, H. Nagino, T. Yamaguchi, H. Kido, I. S. Zavarine, T. Richmond, J. Washington, C. P. Kubiak, *J. Am. Chem. Soc.* **1999**, *121*, 4625−4632.
[21] J. R. Schoonover, G. F. Strouse, *Chem. Rev.* **1998**, *98*, 1335−1355.
[22] J. R. Schoonover, C. A. Bignozzi, T. J. Meyer, *Coord. Chem. Rev.* **1997**, *165*, 239−266.
[23] J. R. Schoonover, G. F. Strousse, R. B. Dyer, W. D. Bates, T. J. Meyer, *Inorg. Chem.* **1996**, *35*, 273−274.
[24] L. C. Abbott, C. J. Arnold, T.-Q. Ye, K. C. Gordon, R. N. Perutz, R. E. Hester, J. N. Moore, *J. Phys. Chem. A.* **1998**, *102*, 1252−1260.
[25] J. R. Schoonover, K. C. Gordon, R. Argazzi, W. H. Woodruff, K. A. Peterson, C. A. Bignozzi, R. B. Dyer, T. J. Meyer, *J. Am. Chem. Soc.* **1993**, *115*, 10996−10997.
[26] J. R. Schoonover, G. F. Strouse, K. M. Omberg, R. B. Dyer, *Comments Inorg. Chem.* **1996**, *18*, 165−188.
[27] W. Kaim, S. Kohlmann, *Inorg. Chem.* **1986**, *25*, 3442−3448.
[28] W. Kaim, S. Ernst, S. Kohlmann, P. Welkerling, *Chem. Phys. Lett.* **1985**, *118*, 431−434.
[29] J. Poppe, M. Moscherosch, W. Kaim, *Inorg. Chem.* **1993**, *32*, 2640−2643.

[30] S. D. Ernst, W. Kaim, *Inorg. Chem.* **1989**, *28*, 1520−1528.
[31] S. M. Scott, A. K. Burrell, P. A. Cocks, K. C. Gordon, *J. Chem. Soc., Dalton Trans.* **1998**, 3679−3684.
[32] C. A. Bignozzi, J. R. Schoonover, F. Scandola, *Prog. Inorg. Chem.* **1997**, *44*, 1−95.
[33] J. Sherborne, S. M. Scott, K. C. Gordon, *Inorg. Chim. Acta* **1997**, *260*, 199−205.
[34] J. Sherborne, K. C. Gordon, *Asian J. Spectrosc.* **1998**, *2*, 137−148.
[35] K. C. Gordon, J. J. McGarvey, *Inorg. Chem.* **1991**, *30*, 2986−2989.
[36] S. M. Scott, A. K. Burrell, K. C. Gordon, *J. Chem. Soc., Dalton Trans.* **1998**, 2873−2877.
[37] K. C. Gordon, J. J. McGarvey, *Chem. Phys. Lett.* **1989**, *162*, 117−122.
[38] M. Schwach, H. D. Hausen, W. Kaim, *Inorg. Chem.* **1999**, *38*, 2242−2243.
[39] W. Kaim, S. Berger, S. Greulich, R. Reinhardt, J. Fielder, *J. Organomet. Chem.* **1999**, *582*, 153−159.
[40] R. J. Crutchley, *Adv. Inorg. Chem.* **1994**, *41*, 273−325.
[41] C. E. G. Evans, M. L. Naklicki, A. R. Rezvani, C. A. White, V. V. Kondratiev, R. J. Crutchley, *J. Am. Chem. Soc.* **1998**, *120*, 13096−13103.
[42] H. Masui, A. L. Freda, M. C. Zerner, A. B. P. Lever, *Inorg. Chem.* **2000**, *39*, 141−152.
[43] A. Klein, E. J. L. McInnes, T. Scheiring, S. Zalis, *J. Chem. Soc., Faraday Trans.* **1998**, *94*, 2979−2984.
[44] N. H. Damrauer, B. T. Weldon, J. K. McCusker, *J. Phys. Chem. A* **1998**, *102*, 3382−3397.
[45] [45a] T. Scheiring, J. Fiedler, W. Kaim, *Organometallics* **2001**, *20*, 1437−1441. [45b] C. S. Campos-Fernandez, R. Clerac, J. M. Koomen, D. H. Russell, K. R. Dunbar, *J. Am. Chem. Soc.* **2001**, *123*, 773−774. [45c] X.-H. Bu, K. Tanaka, M. Shionoya, K. Biradha, H. Morishita, S. Furusho, *Chem. Commun.* **2000**, 971−972. [45d] C. S. Campos-Fernandez, R. Clerac, K. R. Dunbar, *Angew. Chem. Int. Ed.* **1999**, *38*, 3477−3479. [45e] M. Gloeckle, W. Kaim, N. E. Katz, M. G. Posse, E. H. Cutin, J. Fiedler, *Inorg. Chem.* **1999**, *38*, 3270−3274. [45f] P. N. Preston, S. J. Rettig, A. STorr, J. Trotter, *Can. J. Chem.* **1998**, *76*, 1800−1804. [45g] A. Klein, S. Hasenzahl, W. Kaim, J. Fiedler, *Organometallics* **1998**, *17*, 3532−3538. [45h] S. Roche, J. A. Thomas, L. J. Yellowlees, *Chem. Commun.* **1998**, 1429−1430. [45i] W. Kaim, R. Reinhardt, J. Fiedler, *Angew. Chem. Int. Ed. Engl.* **1997**, *36*, 2493−2495. [45j] J. Poppe, M. Moscherosch, W. Kaim, *Inorg. Chem.* **1993**, *32*, 2640−2643. [45k] T. S. Akasheh, Z. M. Al-Ahmad, *Dirasat − Univ. of Jordan, Ser. B* **1990**, *17*, 98−105. [45l] J. G. H. Du Preez, T. I. A. Gerber, M. L. Gibson, *J. Coord. Chem.* **1990**, *22*, 33−42.[45m] W. Kaim, V. Kasack, *Inorg. Chem.* **1990**, *29*, 4696−4699.
[46] S. E. Page, K. C. Gordon, A. K. Burrell, *Inorg. Chem.* **1998**, *37*, 4452−4459.
[47] A. M. Brouwer, R. Wilbrandt, *J. Phys. Chem.* **1996**, *100*, 9678−9688.
[48] A. P. Scott, L. Radom, *J. Phys. Chem.* **1996**, *100*, 16502−16513.
[49] G. A. Guirgis, Y. E. Nashed, J. R. Durig, *Spectrochim. Acta, Part A* **2000**, *56*, 1065−1078.
[50] R. J. H. Clark, T. J. Dines, *Angew. Chem. Int. Ed. Engl.* **1986**, *25*, 131−160.
[51] A. -L. Barra, L. -C. Brunel, F. Baumann, M. Scwach, M. Moscherosch, W. Kaim, *J. Chem. Soc., Dalton Trans.* **1999**, 3855−3857.
[52] P. G. Bradley, N. Kress, B. A. Hornberger, R. F. Dallinger, W. H. Woodruff, *J. Am. Chem. Soc.* **1981**, *103*, 7441−7446.
[53] R. J. Donohoe, C. D. Tait, M. K. DeArmond, D. W. Wertz, *Spectrochim. Acta, Part A* **1986**, *42*, 233−240.
[54] T. G. Spiro, D. S. Caswell, *Inorg. Chem.* **1987**, *26*, 18−19.
[55] K. C. Gordon, J. J. McGarvey, *Chem. Phys. Lett.* **1990**, *173*, 443−448.
[56] J. H. Perng, J. I. Zink, *Inorg. Chem.* **1988**, *27*, 1403−1406.
[57] One pragmatic possibility for the absence of $bptz^{\cdot-}$ features is that the bands observed in **1*** are $bptz^{\cdot-}$ in nature but differ from those seen in $\mathbf{2}^-$ because of the differing λ_{exc} used. The UV/Vis spectroelectrochemistry of $\mathbf{2} \rightarrow \mathbf{2}^-$ reveals that $bptz^{\cdot-}$ is not highly absorbing at 532 or 633 nm.
[58] S. Kohlmann, S. Ernst, W. Kaim, *Angew. Chem.* **1985**, *97*, 698−699; *Angew. Chem. Int. Ed. Engl.* **1985**, *24*, 684−685.
[59] Q. Jaradat, K. Barqawi, T. S. Akasheh, *Inorg. Chim. Acta* **1986**, *116*, 63−73.
[60] W. Kaim, S. Kohlmann, *Inorg. Chem.* **1987**, *26*, 1469−1470.
[61] H. O. House, E. Feng, N. P. Peet, *J. Org. Chem.* **1971**, *36*, 2371−2375.
[62] M. R. Waterland, T. J. Simpson, K. C. Gordon, A. K. Burrell, *J. Chem. Soc., Dalton Trans.* **1998**, 185−192.
[63] The ASTM subcommitte on Raman spectroscopy has adopted eight materials as Raman shift standards (ASTM E 1840). The band wavenumbers for these standards are available at: http://chemistry.ohio-state.edu/~rmccreer/shift.html
[64] R. P. Van Duyne, K. D. Parks, *Chem. Phys. Lett.* **1980**, *76*, 196−200.
[65] C. A. Grant, J. L. Hardwick, *J. Chem. Ed.* **1997**, *74*, 318−321.
[66] M. J. Frisch, G. W. Trucks, H. B. Schlegel, P. M. W. Gill, B. G. Johnson, M. A. Robb, J. R. Cheeseman, T. Keith, G. A. Petersson, J. A. Montgomery, K. Raghavachari, M. A. Al-Laham, V. G. Zakrzewski, J. V. Ortiz, J. B. Foresman, J. Cioslowski, B. B. Stefanov, A. Nanayakkara, M. Challacombe, C. Y. Peng, P. Y. Ayala, W. Chen, M. W. Wong, J. L. Andres, E. S. Replogle, R. Gomperts, R. L. Martin, D. J. Fox, J. S. Binkley, D. J. Defrees, J. Baker, J. P. Stewart, M. Head-Gordon, C. Gonzalez, J. A. Pople, *Gaussian 94, Revision D.4*, Gaussian, Inc., Pittsburgh PA, **1995**.
[67] M. J. Frisch, G. W. Trucks, H. B. Schlegel, G. E. Scuseria, M. A. Robb, J. R. Cheeseman, V. G. Zakrzewski, J. A. Montgomery, Jr., R. E. Stratmann, J. C. Burant, S. Dapprich, J. M. Millam, A. D. Daniels, K. N. Kudin, M. C. Strain, O. Farkas, J. Tomasi, V. Barone, M. Cossi, R. Cammi, B. Mennucci, C. Pomelli, C. Adamo, S. Clifford, J. Ochterski, G. A. Petersson, P. Y. Ayala, Q. Cui, K. Morokuma, D. K. Malick, A. D. Rabuck, K. Raghavachari, J. B. Foresman, J. Cioslowski, J. V. Ortiz, A. G. Baboul, B. B. Stefanov, G. Liu, A. Liashenko, P. Piskorz, I. Komaromi, R. Gomperts, R. L. Martin, D. J. Fox, T. Keith, M. A. Al-Laham, C. Y. Peng, A. Nanayakkara, C. Gonzalez, M. Challacombe, P. M. W. Gill, B. Johnson, W. Chen, M. W. Wong, J. L. Andres, C. Gonzalez, M. Head-Gordon, E. S. Replogle, J. A. Pople, *Gaussian 98*, *Revision A.7*, Gaussian, Inc., Pittsburgh PA, **1998**.
[68] G. Schaftenaar, J. H. Noordik, *J. Comput.-Aided Mol. Design* **2000**, *14*, 123−134.
[69] Computations were performed with the Enraf−Nonius Structure Determination Package, *SDP*, Enraf−Nonius, Delft, **1985**.
[70] G. M. Sheldrick, *SHELXL-95*, Institut für Anorganische Chemie der Universität Göttingen, Germany, **1993**.

Received July 10, 2001
[I01255]